Bioresource Technology 369 (2023) 128443

Contents lists available at ScienceDirect

Bioresource Technology

journal homepage: www.elsevier.com/locate/biortech

Simultaneous removal of nitrate and ammonium by hydrogen-based partial denitrification coupled with anammox in a membrane biofilm reactor

Si Pang [a,b], Yun Zhou [c], Lin Yang [a,b], Jingzhou Zhou [a,b], Xiaodi Li [a,b], Siqing Xia [a,b,*]

[a] State Key Laboratory of Pollution Control and Resource Reuse, College of Environmental Science and Engineering, Tongji University, Shanghai 200092, China
[b] Shanghai Institute of Pollution Control and Ecological Security, Shanghai 200092, China
[c] College of Resources and Environment, Huazhong Agricultural University, Wuhan 430070, China

HIGHLIGHTS

- A novel H_2-PDA process was developed for removal of nitrate and ammonium.
- An effluent TN of 2.6 mg/L and an effluent TOC of 0.7 mg/L were achieved.
- DP and AP were responsible for 6.3% and 93.7% of TN removal, respectively.
- *Candidatus_Brocadia* was predominant in TN removal in H_2-PDA process.
- The up-regulation of S-methylhGSH played a key role in TN removal in H_2-PDA process.

GRAPHICAL ABSTRACT

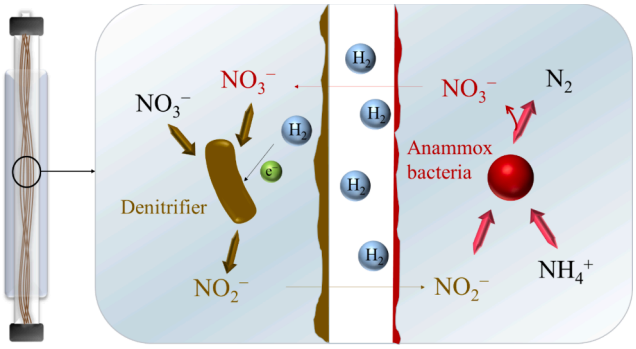

ARTICLE INFO

Keywords:
Hydrogen-based partial denitrification coupled with anammox (H_2-PDA)
Membrane biofilm reactor (MBfR)
Nitrate and ammonium removal
Microbial community
Metabonomics

ABSTRACT

Hydrogen-based membrane biofilm reactors (MBfRs) are effective for nitrogen removal. However, the safety of hydrogen limited the application of MBfR. Here, a hydrogen-based partial denitrification system coupled with anammox (H_2-PDA) was constructed in an MBfR for reducing hydrogen demand significantly. The metabolomics and structures of microbial communities were analyzed to determine the phenotypic differences and drivers underlying denitrification, anammox, and H_2-PDA. These findings indicated that total nitrogen (TN) removal increased from 57.1% in S1 to 93.7% in S2. During the H_2-PDA process, partial denitrification and anammox contributed to TN removal by 93.7% and 6.3%, respectively. Community analysis indicated that the H_2-PDA system was dominated by the genus *Meiothermus*, which is involved in partial denitrification. Collectively, these findings confirmed the feasibility of incorporating the H_2-PDA process in a MBfR and form a foundation for the establishment of novel and practical methods for efficient nitrogen removal.

* Corresponding author at: State Key Laboratory of Pollution Control and Resource Reuse, College of Environmental Science and Engineering, Tongji University, Shanghai 200092, China.
E-mail address: siqingxia@tongji.edu.cn (S. Xia).

https://doi.org/10.1016/j.biortech.2022.128443
Received 20 October 2022; Received in revised form 29 November 2022; Accepted 1 December 2022
Available online 5 December 2022

1. Introduction

The anammox process is a promising autotrophic nitrogen removal technology that requires no aeration or organic carbon sources and minimizes sludge production (Gu et al., 2018). However, the occurrence of residual nitrate (NO_3^--N) in effluents and access to nitrite (NO_2^--N) sources are important challenges in the development and practical application of anammox. Therefore, anammox coupled with partial denitrification (PDA) has significant advantages for nitrogen removal (Du et al., 2020a).

During the PDA process, NO_3^--N first receives electrons from electron acceptors and is converted into NO_2^--N by nitrate reductase through partial denitrification (Moreno-Vivian et al., 1999). Anammox bacteria then transform influent ammonia (NH_4^+-N), together with NO_2^--N, into gaseous nitrogen (N_2) through oxidation (Kuenen, 2008). Moreover, denitrifying bacteria continue to reduce anammox-produced NO_3^--N into NO_2^--N, allowing continuous exploitation by anammox bacteria until it becomes completely depleted (Du et al., 2020a). Partial denitrification can be achieved by the maintenance of a suitable balance between chemical oxygen demand and nitrogen, specifically, the COD/N ratio (Gong et al., 2013). However, the addition of carbon sources such as methanol during partial denitrification not only potentially leads to secondary organic pollution but also presents difficulties for the coexistence of autotrophic and heterotrophic microorganisms within a single reactor (Chen et al., 2018).

Hydrogen (H_2)-derived membrane biofilm reactors (MBfRs) can reduce NO_3^--N without organic compounds and have been used to successfully achieve autotrophic partial denitrification (Pang et al., 2022). Furthermore, previous studies have reported that efficient delivery of the electron donor (H_2) through hollow fiber membranes can be achieved using a gas regulator (Tang et al., 2011). H_2 is not only non-toxic but also far more cost-effective than other electron donors, in addition to achieving low biomass yields without residues in the bioreactor (Tang et al., 2011). Therefore, the incorporation of H_2-based partial denitrification coupled with anammox (H_2-PDA) in MBfRs provides a novel and efficient means for nitrogen removal and broadens the practical application of MBfRs.

Recently, metabolomic studies were conducted to characterize the dynamics of denitrifiers and anammox bacteria (Feng et al., 2018) to gain insights into the molecular pathways involved in nitrogen metabolism (Tautenhahn et al., 2012). Notably, these studies have demonstrated the involvement of specific metabolic routes for denitrifying autotrophic/heterotrophic bacteria (Bai et al., 2022). Feng et al. (2018) identified such activation of metabolic pathways associated with amino and nucleotide sugar production in annamox bacteria, resulting in the secretion of additional extracellular polysaccharides. Although numerous annamox-associated metabolic pathways have been identified (Guven et al., 2005), there appear to have been no previous studies addressing the PDA process from a metabolomics perspective.

Thus, the aims of this study were to (1) devise a novel H_2-PDA process in MBfR; (2) explore the microbial community succession in the H_2-PDA; (3) identify variations in nitrogen removal mechanisms via metabolomics analysis. Mass balance assessments were performed to determine the calculate the respective influence by partial denitrification/anammox to for extracting nitrogen. Such results provide insight into the molecular mechanisms that drive the H_2-PDA process, in addition to offering a viable alternative for deep nitrogen removal.

2. Materials and methods

2.1. Reactor settings

A 60-mL MBfR (Fig. 1) was run continuously for 128 days. The MBfR was installed with main and sampling column membrane modules. Each membrane module contained 30 non-porous polypropylene hollow-fibers having outer diameters at 200 μm and inner diameters at 100 μm (Teijin, Ltd., Tokyo, Japan) and lengths of 28 cm for ultra-pure (>99.999 %) H_2 delivery. A gas pipeline was connected to the H_2-gas tank, and the pressure was regulated by a regulator at the end of the gas pipeline. The lumen pressure was constant at 0.02 MPa, measured by a gas gauge.

A feed-pump (BT100-2J®, Longerpump™, Baoding, China) supplied

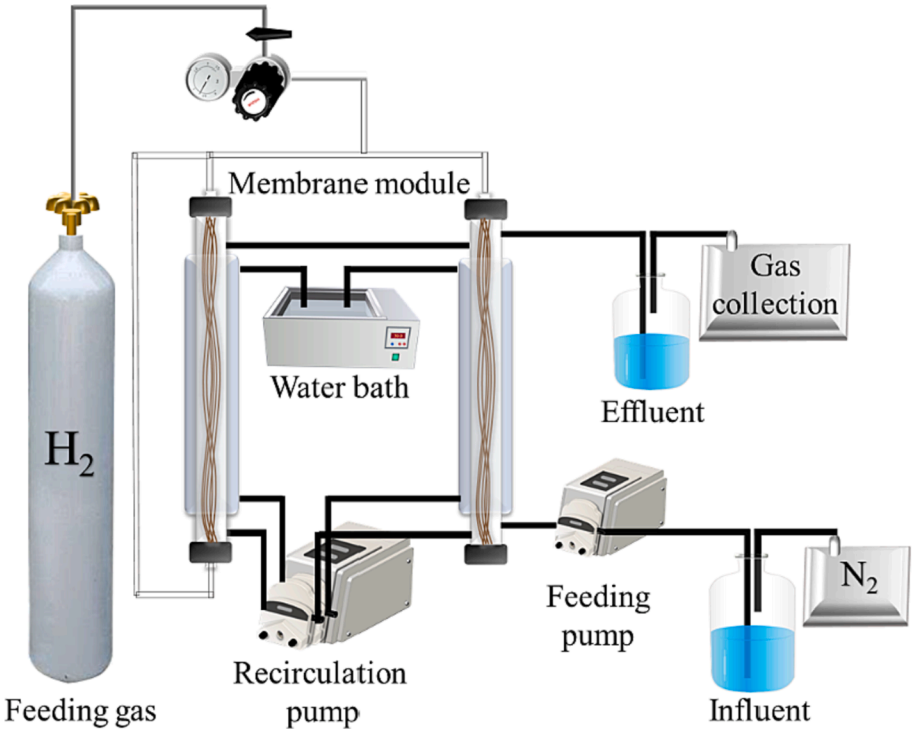

Fig.1. Schematic of the continuous operated H_2-based membrane biofilm reactor (MBfR) using polypropylene hollow-fiber membranes.

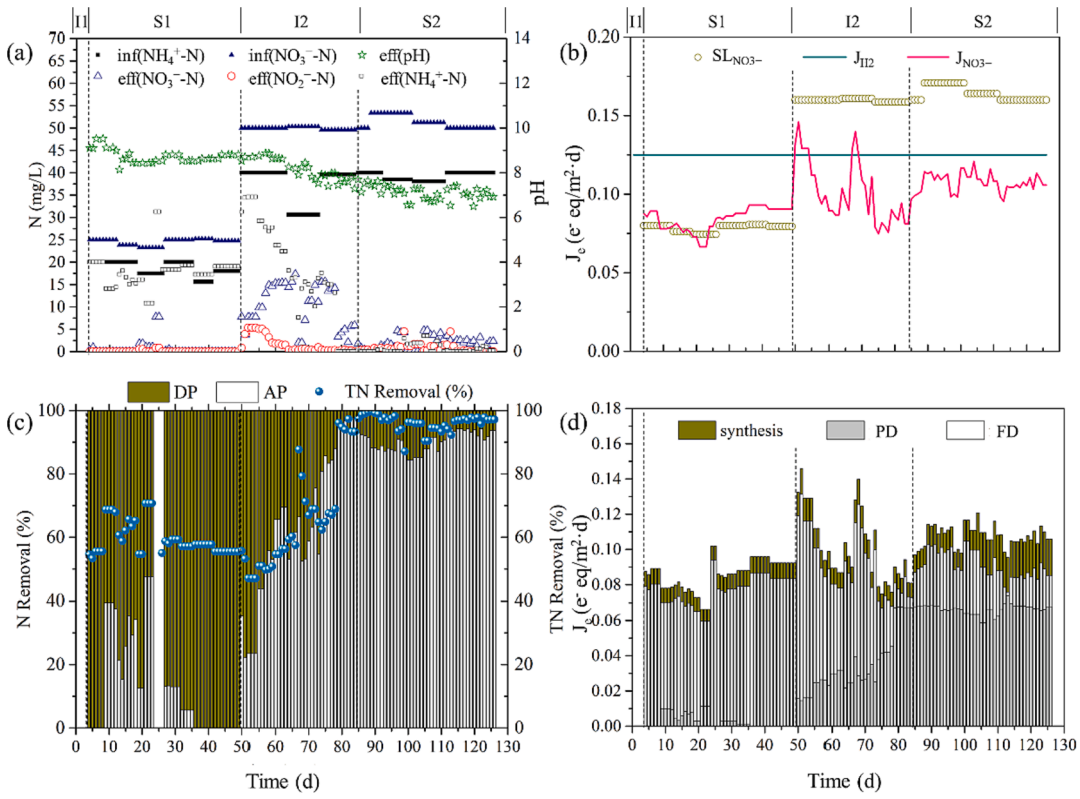

Fig. 2. Performance of the MBfR for treatment stages I1, S1, I2, and S2: (a) Concentrations of NO_3^--N, NH_4^+-N and NO_2^--N, along with effluent pH; (b) Calculated maximum H_2 supply flux (J_{H2}), NO_3^--N surface loading flux (SL_{NO3-}), and maximum NO_3^--reduction consumption flux (J_{NO3-}); (c) Contributions of anammox proportion (AP) and denitrification proportion (DP) to N removal, as well as TN removal; (d) Hydrogen electron-flow towards biomass synthesis, partial denitrification (PD) and full denitrification (FD).

synthetic wastewater to the MBfR at an influent flow rate of 0.09 mL/min. A recirculating-pump provided reactor mixing (BT100-2 J®, Longerpump™) (rate = 64.8 mL/min); the bath water (maintained at 30 °C) was recirculated using the same recirculation pump. The influent pH was manually optimized through 1 M HCl or NaOH to maintain pH 7.4 ± 0.5.

2.2. Synthetic wastewater and operational strategies

A 5-L glass bottle was used for preparation of the influent, which was then sparged with 100 % gaseous N_2 (ten minutes) for eliminating dissoluted oxygen (DO). Further oxygen was prevented from entering the bottle by the connection of a N_2-containing Tedlar bag.

The operation comprised two inoculation stages (I1 and I2) and two operation stages (S1 and S2). The H_2-PDA process was initiated as follows (Table 1):

I1: 20 mL of denitrifying sludge (mixed liquor suspended solids (MLSS) 5.3 g/L), which was obtained from an MBfR with 68 % nitrite transformation rate (Pang et al., 2022), was inoculated into the MBfR in this study. The internal circulation was operated in batch mode for three days (Day 1–3) to enable biomass attachment to the surfaces of the hollow fiber membranes.

S1: The reactor was operated continuously for 45 days (Day 4–48). The hydrogen autotrophic denitrifying biofilm was stabilized, as the level of effluent NO_3^--N remained below 2 mg/L for 10 consecutive days. The synthetic wastewater used in S1 had the following composition: $NaNO_3$-N, 25 mg/L; NH_4Cl-N, 20 mg/L; $NaHCO_3$, 80 mg/L; $CaCl_2{\cdot}2H_2O$, 100 mg/L; $MgSO_4{\cdot}7H_2O$, 100 mg/L; KH_2PO_4, 40 mg/L; 36 % HCl, 7 mL/L; $FeCl_2{\cdot}4H_2O$, 1.5 g/L; $CoCl_2{\cdot}6H_2O$, 0.19 g/L; $MnCl_2{\cdot}4H_2O$, 0.1 g/L; $ZnCl_2$, 70 mg/L; H_3BO_3, 6 mg/L; $Na_2MoO_4{\cdot}2H_2O$, 36 mg/L; $NiCl_2{\cdot}6H_2O$, 24 mg/L; $CuSO_4{\cdot}5H_2O$, 3 mg/L; NaOH, 0.5 g/L; $Na_2SeO_3{\cdot}5H_2O$, 9 mg/L; $Na_2WO_4{\cdot}2H_2O$, 8 mg/L.

Table 1
Operational strategies during the long-term experiment.

Stage	Period (days)	NH + 4-N (mg N/L)	NO−3-N (mg N/L)	TN loading rate (g N/(L·d))	Operational modes	Purposes
I1	0–3	/	/	/	Batch mode	To build up denitrification biofilm
S1	4–25	20	25	0.1	Continuous mode	To stabilize full denitrification process
I2	26–64	40	50	0.2	Batch/ Continuous mode	To attach anammox on the established biofilm surface
S2	65–104	40	50	0.2	Continuous mode	To achieve one-stage nitrogen removal

I1, Inoculation 1; S1, Stage 1; I2, Inoculation 2; S2, Stage 2.

I2: The reactor was run in a designed procedure for 35 days (Day 49–83) with high concentrations of synthetic wastewater (Table 1). In the first day of the procedure, 10-mL of anammox inoculum was added into the MBfR, and the MBfR was run in the batch mode for the attachment of anammox bacteria, then the MBfR was fed with continuous influent in the next two days. The inoculation process was repeated until the rate of total nitrogen (TN) removal exceeded 90 %. The anammox inoculum (MLSS 1.1 g/L) was obtained from an anammox membrane bioreactor (MBR) with 50 mg/L NH_4^+-N influent (Cai et al., 2022). The pH value, temperature, and hydraulic retention time (HRT)

in anammox MBR were controlled at 7.4, 36.5 °C, and 19.0 h, respectively.

S2: The MBfR was run with a continuous supply of influent for 45 days (Day 84–128) to determine whether the H_2-PDA process was stable. The wastewater used in I2 and S2 contained the following: $NaNO_3$-N, 50 mg/L; NH_4Cl-N, 40 mg/L; $NaHCO_3$, 150 mg/L; $CaCl_2{\cdot}2H_2O$, 200 mg/L; $MgSO_4{\cdot}7H_2O$, 200 mg/L; KH_2PO_4, 40 mg/L; 36 % HCl, 7 mL/L; $FeCl_2{\cdot}4H_2O$, 1.5 g/L; $CoCl_2{\cdot}6H_2O$, 0.19 g/L; $MnCl_2{\cdot}4H_2O$, 0.1 g/L; $ZnCl_2$, 70 mg/L; H_3BO_3, 6 mg/L; $Na_2MoO_4{\cdot}2H_2O$, 36 mg/L; $NiCl_2{\cdot}6H_2O$, 24 mg/L; $CuSO_4{\cdot}5H_2O$, 3 mg/L; NaOH, 0.5 g/L; $Na_2SeO_3{\cdot}5H_2O$, 9 mg/L; $Na_2WO_4{\cdot}2H_2O$, 8 mg/L.

2.3. Chemical analysis of samples

Influent/effluent aliquots were immediately passed through 0.22 μm filters (Millipore™) having polyether sulfone (PES) membranes, followed by measurement of the pH. Samples were kept at 4 °C and were processed within the following three days. NO_3^--N/NO_2^--N levels were determined through standardized protocols (APHA, 2017) and pH/DO were determined through portable pH and DO meters, respectively (HQ40d, HACH, Loveland, CO, USA). All measurements were conducted in triplicate. Inorganic carbon together with total organic carbon (TOC) levels were evaluated using a TOC analyzer (TOC-L®, Shimadzu™, Japan).

Fiber samples were obtained on S1 and S2 termination. Afterward, 1-cm-long sections of biofilm fiber were cut using sterilized scissors from the fiber bundle. The fiber was fixed through glutaraldehyde (2.5 % in 0.1 mol/L phosphate buffer, pH 7.4) concerning scanning electron microscopic analyses (SEM; Zeiss Sigma 300, Germany). Biofilm samples were collected in triplicate during the last 10 days of the experiment at stages S1 and S2. Parts of the biofilm samples were stored at −80 °C in a centrifugal tube for metabolomics detection. Other biofilm aliquots were flash-frozen within liquid nitrogen before DNA and RNA collection.

2.4. Isolation and analysis for extracellular polymeric substances (EPS)

EPS was isolated with a heating method. The collected biofilms were washed, and samples were resuspended to 5 mL + saline solution (0.05 % [w/v] NaCl in water). The samples were heated (60 °C/thirty minutes) followed by centrifugation (12 000 rpm/fifteen minutes). Supernatants required filtering across 0.45-μm filters to obtain filtrate EPS.

Three-dimensional excitation-emission matrix (3D-EEM) fluorescence analysis of EPS samples at the end of stage S1 and S2 was performed on a fluorescence photometer (F-4600®, Hitachi™, Japan).

2.5. Extraction of DNA and RNA and reverse transcription of RNA

Microbial DNA and RNA were isolated with PowerBiofilm DNA and RNA Isolating kits (Mo Bio Laboratories™, Carlsbad, CA, USA), respectively, following provided protocols. RNA was rapidly converted into cDNA using PrimeScript® RT Reagent Kit (Takara™, China), according to provided instructions, and stored at −80 °C before quantitative real-time PCR (qPCR) analysis.

2.6. Microbial community analysis

The anammox genes were assessed in triplicate using a CFX96 Touch® real-time PCR Detection System (Bio-Rad™, Hercules, CA, USA). Functional genes were amplified using the SYBR-Green method. The Amx368F (5′-TTC GCA ATG CCC GAA AGG-3′) and Amx820R (5′-AAA ACC CCT CTA CTT AGT GCC C-3′) primers amplified anammox 16S rRNA genes (Schmid et al., 2003) using a previously described protocol (Pang et al., 2022).

DNA was sequenced by Shanghai Majorbio Technology™ (Shanghai, China) on an Illumina™ MiSeq® system. The primers and sequencing procedures have been described previously (Xia et al., 2020).

2.7. Metabolomic analysis

Untargeted metabolomic analysis of the biofilm samples (S1 and S2) and the anammox inoculum (An) was performed by Shanghai Majorbio Technology. The metabolite extraction and detection procedures were described previously (Feng et al., 2018). Briefly, metabolite extraction was conducted at a low temperature by adding extraction solution based on the sample quantity. The supernatant of the metabolite solvent was centrifuged for liquid mass spectrometry detection. Progenesis QI® software (Waters Corporation™, USA) was used in peak extraction, alignment, and identification. Data matrices, including peak areas, retention times, mass/charge ratios, and compound identification, were obtained and used for post-processing and bioinformatics.

Liquid chromatography-mass spectrometry (LC-MS) was performed through UHPLC-Q Exactive HF-X® system (ThermoFisher™, USA) using an ACQUITY UPLC HSS T3® column (100 mm × 2.1 mm I.D., 1.8 μm; Waters™, USA). The mobile phases A and B contained 95 % water + 5 % acetonitrile (harboring 0.1 % formic acid), and 47.5 % acetonitrile + 47.5 % isopropanol + 5 % water (harboring 0.1 % formic acid), respectively. Aliquot size and column temperature were 2 μL and 40 °C, respectively. Quality control (QC) samples of the same volumes as the target samples were a mixture of equal volumes of sample extracts (10 μL). QC samples were run after every 5–15 samples during the analysis.

2.8. Calculations and statistical analysis

The respective contributions of the anammox proportion (AP) and denitrification proportion (DP) to TN removal were examined from previous procedures (Zhang et al., 2022).

$$AP = \frac{\left[\mathrm{inf}\left(NH_4^+\right) - \mathrm{eff}\left(NH_4^+\right)\right] + 1.32\left[\mathrm{inf}\left(NH_4^+\right) - \mathrm{eff}\left(NH_4^+\right)\right]}{\mathrm{inf}(TN) - \mathrm{eff}(TN)} \times 100\% \quad (1)$$

$$DP = \frac{\left[\mathrm{inf}\left(NO_3^-\right) - \mathrm{eff}\left(NO_3^-\right)\right] - 1.32\left[\mathrm{inf}\left(NH_4^+\right) - \mathrm{eff}\left(NH_4^+\right)\right] + 0.26\left[\mathrm{inf}\left(NH_4^+\right) - \mathrm{eff}\left(NH_4^+\right)\right]}{\mathrm{inf}(TN) - \mathrm{eff}(TN)} \times 100\% \quad (2)$$

The maximum H_2 flux was determined by the methods of Tang et al. (2011):

$$J_{H_2} = D_m \frac{k_m}{z_m} K_L P_0 \left(\frac{d_m - z_m}{d_m}\right) \quad (3)$$

where D_m is H_2-diffusion coefficient in the membrane (1.4×10^{-7} m^2/d for polypropylene fibers), k_m is H_2 solubility coefficient in the membrane (1.29 m^3 H_2 at standard temperature and pressure/m^3 membrane bar), K_L is coefficient that converts H_2 from volume to mass (1 g/0.0112 m^3 at standard temperature and pressure), P_0 is the absolute H_2 pressure in the hollow-fiber lumen (bar), d_m is hollow-fiber outer diameter (200 μm for polypropylene fibers), and z_m is membrane thickness (50 μm for polypropylene fibers).

The NO_3^--N surface loading flux (SL_{NO3-}), consumption flux (J_e) and N balances were determined by the methods of Pang et al. (2022):

$$SL_{NO3-} = \frac{QS^0}{aV} \quad (4)$$

$$J_e = \frac{Q\alpha(S^0 - S)}{aV} \quad (5)$$

$$J_{NO3-} = J_{PD} + J_{FD} + J_{synthesis} \quad (6)$$

where Q is the influent flow rate in m^3/d and S^0 is the influent concentration of the acceptor (g N/m^3). a is the specific surface area (m^{-1}), and V is the reactor volume (m^3). The value of α depends on the extent to which NO_3^- is reduced: the ratios (in g H_2/g N) are 0.36 and 0.14 for reductions to N_2 and NO_2^-, respectively, when biomass synthesis is not considered. Based on the equations of full denitrification and partial denitrification, the values of α in biomass synthesis are 0.06 and 0.03 for reductions to N_2 and NO_2^-, respectively (Rittmann and McCarty, 2020).

Metabolomic datasets were assessed across Majorbio Cloud Platform (https://www.majorbio.com). Pearson correlation coefficients and analysis of variance (ANOVA) were determined through SPSS (V. 25.0). Differences with an adjusted $p < 0.05$ were deemed to confer statistical significance.

3. Results and discussion

3.1. H_2-PDA performance

Here, denitrification was studied in a MBfR system (I1 and S1). In stage S1, the NO_3^--N together with NO_2^--N effluents were identified as stable at 0.2 mg/L and 0.0 mg/L, accordingly, indicating that the MBfR could be used for partial denitrification as previously shown (Pang et al., 2022). The effluent pH increased to 8.1–9.5 due to the strong bases produced during full denitrification. Throughout this stage, the contribution of DP reached 100 %, but the TN removal was approximately 57.7 % because of the absence of anammox bacteria.

Considering that the inoculated microorganisms in I1 have been acclimatized by partial denitrification, the loading rate of TN was increased from 0.1 g N/(L·d) to 0.2 g N/(L·d) in stage I2, so that partial denitrification can be achieved in the cases of H_2 shortage conditions (Pang et al., 2022). Inoculation of anammox bacteria in I2 led to a reduction from 34.4 mg/L to 0.3 mg/L within effluent NH_4^+-N, having a reduction in pH from 8.7 to 7.7 in the effluent. The decrease of effluent pH was attributed to the transition from full denitrification to partial denitrification, which produced very few strong bases (Rittmann and McCarty, 2020). Therefore, the effluent pH can be used as an indicator of H_2-PDA in MBfR.

Given that the H_2-PDA process was achieved at the end of I2, inoculation was stopped to investigate the stabilization of H_2-PDA in the MBfR. In S2, NH_4^+-N removal increased to 99.5 % with 95.4 % NO_3^--N removal (see supplementary material). During this stage, the TN removal rate stabilized at > 90 %, as described in a previous study on the PDA process (Du et al., 2020a). Additionally, the electrons consumed by PD in S2 (0.06–0.07 e^- eq/(m^2·d)) were significantly higher than in S1 (0.00–0.01 e^- eq/(m^2·d)), which provided higher nitrite for anammox, thus contributed to TN removal in S2. N balanced (see supplementary material) showed that the influent TN was removed from the water in the form of N_2 instead of NO_2^--N, thus, AP contribution was raised to 93.7 % while DP decreased to 6.3 %. Furthermore, in the case of higher TN removal in S2, the overall electron consumption in S2 (0.10–0.12 e^- eq/(m^2·d)) was close to that in S1 (0.07–0.09 e^- eq/(m^2·d)), which proved that H_2-PDA greatly decreasing H_2 consumption. On the one hand, the lower electron consumption was consistent with earlier reports (Van Ginkel et al., 2012) that described reduced H_2 safety risks. One the other hand, the removal of NH_4^+-N broadened the application of MBfR.

3.2. Dynamics of biofilm structure and function

The microorganisms in the denitrifying biofilm were mainly *bacilli* (see supplementary material), along with some *cocci* and *hyphomycetes*. Furthermore, significant EPS accumulation was seen on the surfaces and insides of the denitrifying biofilm. These results showed a similar structure with the reported PD granular sludge (Du et al., 2020b), which provided a basis for the achievement of the PD process.

During stage S2, the number of *cocci* increased. According to the size of the anammox bacteria (Kuenen, 2008), this could be the result of inoculation of anammox. It is worth noting that the morphological characteristics in stage S2 included lumps, with a clearer hierarchy than in the denitrifying biofilm (see supplementary material). Moreover, the high aggregation ability of bacteria is determined by the stronger hydrophobic characteristics in anammox EPS (Hou et al., 2015). Furthermore, down-regulation of metabolic pathways associated with amino and nucleotide sugar production were observed in autotrophic anammox consortia (Feng et al., 2018), leading to significantly reduced EPS in H_2-PDA biofilms.

The abundance and expression of anammox 16S rRNA genes were characterized for further identification of the anammox bacteria in Stages S1 and S2. Although the abundance of anammox genes was 1087 copies/g biofilm, no expression was detected. During stage S2, both the present abundance (amplified from DNA) and expressed abundance (amplified from RNA) of anammox genes increased significantly to 5.4×10^6 and 4.7×10^6 copies/g biofilm, respectively.

3.3. Microbial community analysis

3.3.1. Community structures at the phylum and class levels

In the full denitrification stage (S1), the dominant phylum was Proteobacteria (93.7 %, see supplementary material), including Gammaproteobacteria (81.8 %) and Alphaproteobacteria (11.9 %) (see supplementary material). This agrees with previous reports that Proteobacteria are the most common phylum seen in denitrification processes (Yuan et al., 2022). In the H_2-PDA process (S2), the abundance of Proteobacteria decreased to 38.5 %, whereas that of Deinococcota increased from 0 % to 39.9 %. Deinococcota were abundant in anammox granules (Lu et al., 2021) and sulfur autotrophic partial denitrification (Yuan et al., 2022), which was consistent with the H_2-PDA process in stage S2. Other abundant phyla were Firmicutes, Bacteroidota, Desulfobacterota, Myxococcota, and Chloroflexi, all of which were more abundant in S2 (accounting for 6.0 %, 5.5 %, 4.3 %, 1.7 %, and 1.1 %, respectively) than in S1 (accounting for 2.7 %, 1.3 %, 0.0 %, 0.0 %, and 0.4 %, respectively). Therefore, these findings indicated that the H_2-PDA process enriched these phyla, consistent with previous observations (Chu et al., 2015). Firmicutes play major roles in the decomposition of organic materials (Wrighton et al., 2008). Therefore, the elevated abundance of Firmicutes could explain the reduction in the concentration of effluent TOC (see supplementary material).

Only eight classes were abundant (>1% within one aliquot minimum) within two biofilm aliquots (see supplementary material). Among these classes, Gammaproteobacteria and Alphaproteobacteria were more abundant in stage S1 (accounting for 81.8 % and 11.9 %, respectively) than in S2 (accounting for 36.3 % and 2.2 %, respectively), indicating that these taxa were primarily involved in the denitrification process. The abundance of Bacteroidia increased from 1.3 % to 4.8 % during S2. Similarly, Bacteroidia was also abundant (9.6 %) during sulfidation anammox processes and was responsible for denitrification in this process.

3.3.2. Genus-level community structures

Fig. 3 illustrates composition and distribution of key genera (genera with relative abundances >1 % in at least one sample) and cluster analysis of functional bacteria based on Pearson similarity. According to the results of cluster analysis, 19 key genera were divided into four

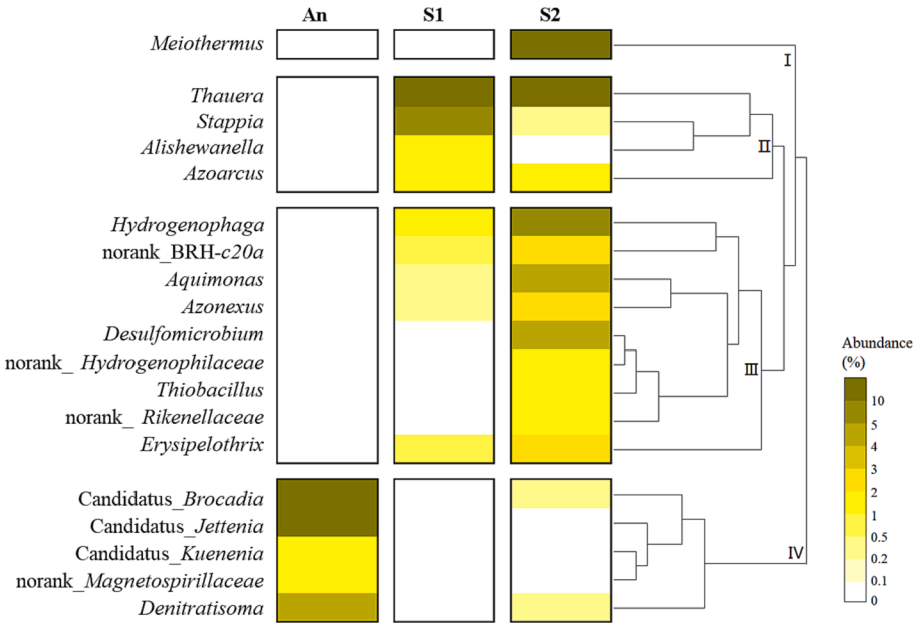

Fig. 3. Heat map of the 19 key genera (abundance >1 % in at least one sample) clustered based on Pearson similarity. An, anammox inoculum; S1, biofilm samples in stage S1; S2, biofilm samples in stage S2.

groups: (1) *Meiothermus* was in Group I, which only existed in S2 and showed the highest abundance (39.9 %); (2) the abundances of *Thauera, Stappia, Alishewanella*, and *Azoarcus* in Group II was generally higher during S1 than during S2; (3) Group III contained *Hydrogenophaga, Aquimonas, Desulfomicrobium, Azonexus,* norank_BRH-*c20a*, *Erysipelothrix, Desulphorus, Desulphorus, Desulphorus, Desulphorus, Desulphorus*, and *Desulphorus*. The abundances of these genera in S2 were generally higher than in S1. (4) Group IV contained *Candidatus_Brocadia, Candidatus_Jettenia, Candidatus_Kuenenia,* norank_*Magnetospirillaceae*, and *Denitratisoma*, which were the main genera in the anammox inoculum for effective anammox functioning (Cheng et al., 2020).

Members of the *Meiothermus* genus can secrete laccase, which can reduce effluent viscosity (Perna et al., 2019). Therefore, the EPS attached to the biofilm in stage S2 was decomposed by *Meiothermus*, thus decreasing the effluent TOC (see supplementary material). Furthermore, *Meiothermus* was dominant in hydrogen autotrophic denitrification (Dong et al., 2021), resulting in NO_3^--N removal in the MBfR (Lai et al., 2018). Furthermore, a significant increase in S2 indicated that *Meiothermus* played an important role in partial denitrification. *Thauera, Stappia, Alishewanella,* and *Azoarcus* are all typical denitrifying functional bacteria (Averill and Tiedje, 1982; Cao et al., 2017), and their abundances in the H_2-PDA process (S2) decreased from 74.8 %, 8.1 %, 1.9 %, and 1.3 % to 15.5 %, 0.2 %, 0.0 %, and 1.0 %, respectively, which resulted from the transition from full denitrification to partial denitrification. Although *Thauera* was reported to participate in H_2-denitrification (Pang et al., 2022), the competition with anammox bacteria decreased its abundance (Li et al., 2022). *Hydrogenophaga*, norank_*Hydrogenophilaceae*, *Desulfomicrobium,* and *Thiobacillus* are also microorganisms with denitrification function (Xia et al., 2020). Their increased abundances in stage S2 (7.3 %, 1.6 %, 4.2 %, and 1.8 %, respectively) were indicative of their involvement in partial denitrification. Collectively, *Meiothermus*, *Hydrogenophaga*, norank_*Hydrogenophilaceae*, *Desulfomicrobium,* and *Thiobacillus* were mainly in charge of the H_2-denitrification in H_2-PDA process.

Although three kinds of typical anammox bacteria (*Candidatus_Brocadia* (15.9 %), *Candidatus_Jettenia* (71.7 %), and *Candidatus_Kuenenia* (1.8 %)) were abundant within anammox inoculum, only *Candidatus_Brocadia* established itself in the MBfR (0.45 %). Recent studies on total nitrogen removal via the PDA process confirmed the low abundance of anammox bacteria (~0.58 %) treated with NH_4^+-N at 58.3 mg/L (Du et al., 2016), and 0.45 % *Candidatus_Brocadia* treated with 40 mg/L NH_4^+-N in the present investigation.

The evolution of the 19 key genera observed in this study was investigated by construction of a phylogenetic tree (see supplementary material). Considering that uncultured_BRH-*c20a* was capable of CO_2 fixing (Jiang et al., 2020), incidence describing *Candidatus_Brocadia, Candidatus_Jettenia*, together with *Candidatus_Kuenenia* sharing the same root with norank_BRH-*c20a* indicated that anammox bacteria were also important in inorganic carbon fixing. norank_*Magnetospirillaceae* had the same root with *Stappia*, indicating that norank_*Magnetospirilla* was also capable of denitrification (Yuan et al., 2021). Similarly, norank_*Hydrogenaceae* was closely related to *Thiobacillus,* showing that norank_*Hydrogenaceae* was a kind of denitrifying bacteria capable of sulfate reduction similar to *Thiobacillus* (Kiskira et al., 2017).

3.4. Microbial metabolic analysis

3.4.1. Differences in EPS secretion resulting from metabolic conversion

For the EPS secreted by biofilms (Fig. 4a and b), tryptophan-like proteins, fulvic acid, and humic acid were detected in S1, but only tryptophan-like proteins were detected in S2. Furthermore, the signal intensity of tryptophan-like proteins in S2 was lower than that in S1, which was consistent with the low amounts of organic material seen in the S2 effluent (see supplementary material). Therefore, the H_2-PDA process not only improved the removal of total nitrogen but also contributed to the reduction of TOC. Tryptophan-like proteins, fulvic acid, and humic acid are the principal EPS components, although their secretory mechanisms differ. Proteins secreted by bacteria are closely associated with both the aggregation of consortia and biofilm production (Jia et al., 2017). Nine amino acids were identified (see supplementary material), significantly fewer than the 18 observed in mixotrophic anammox consortia (Feng et al., 2018). The amino acid contents decreased in S2, resulting in a decrease of effluent protein (Fig. 4). These findings were inconsistent with those of Feng et al. (2018), who observed that protein secretion was stimulated by the presence of organic carbon, indicating the high cleanability of H_2-PDA.

The top-30 metabolites with the highest metabolic abundance in S1 and S2 are illustrated in Fig. 4c, which was divided into two groups by

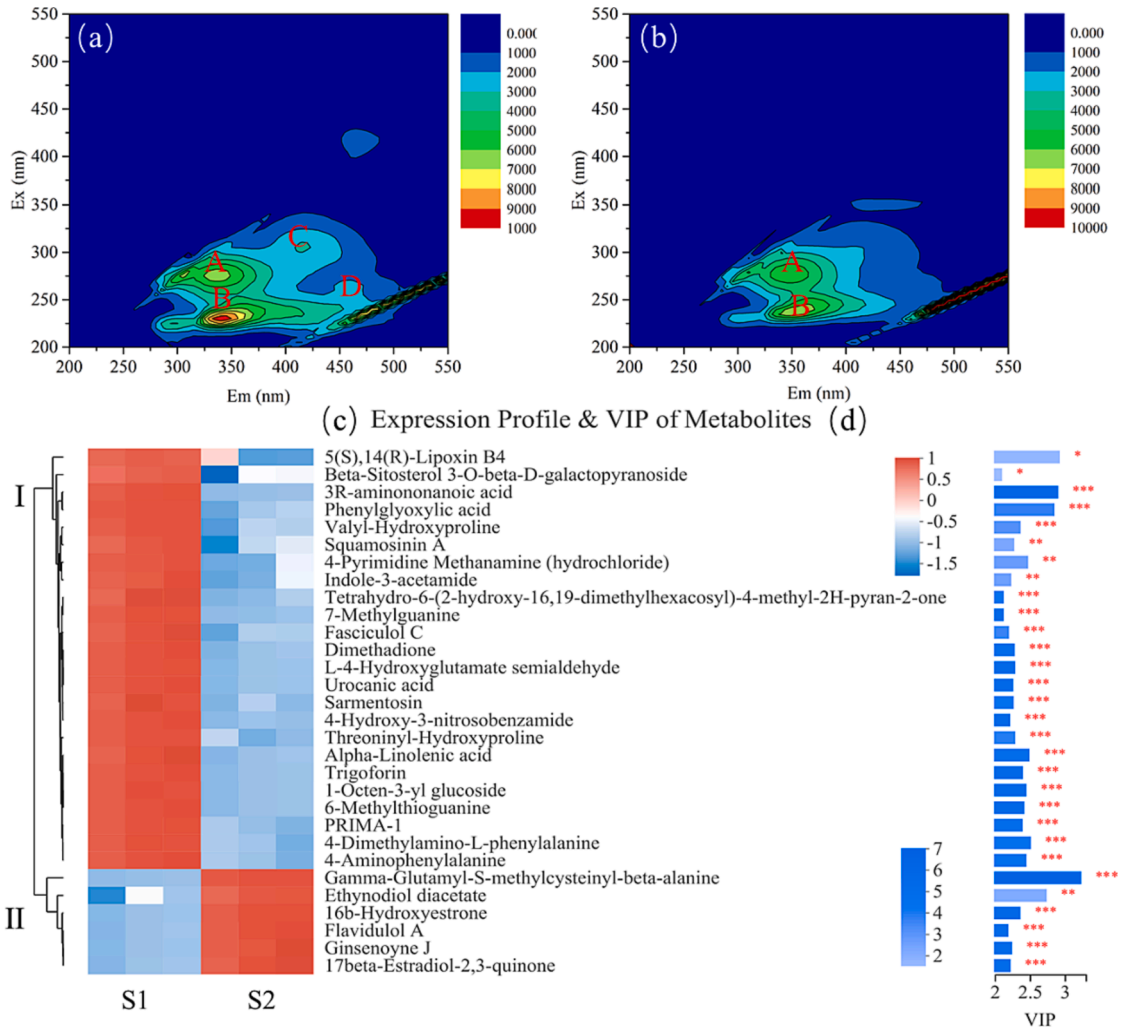

Fig. 4. 3D-EEM of the effluent in (a) S1 and (b) S2 (A, B-tryptophan protein; C-fulic acid; D-humic acid). The heat map of (c) Top30 metabolites in abundance and (d) the related VIP values.

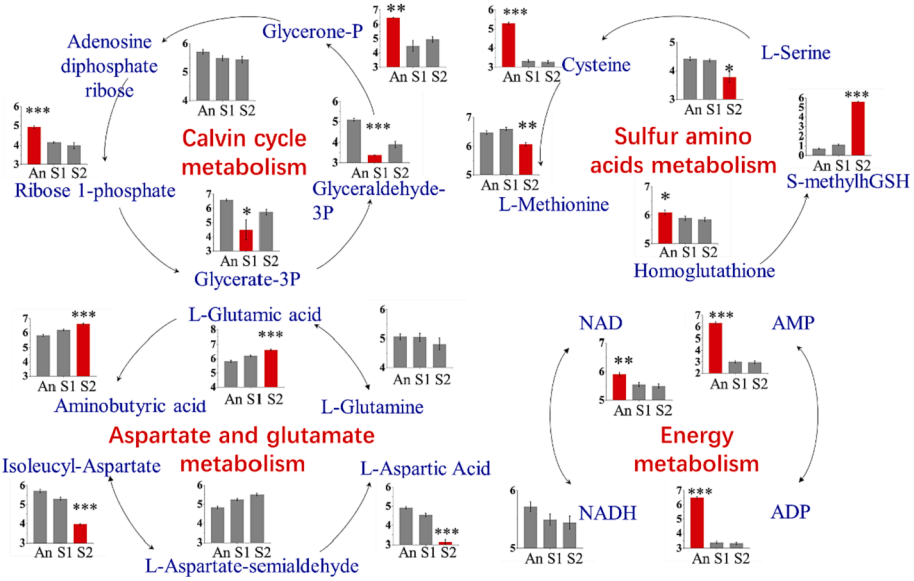

Fig. 5. Metabolomic abundance for anammox (An) and biofilm samples (S1 and S2). Red indicates significant changes (*, $p < 0.05$; **, $p < 0.01$; ***, $p < 0.001$). S-methylhGSH: gamma-glutamyl-S-methylcysteinyl-beta-alanine, NAD: nicotinamide adenine dinucleotide, NADH: reduced form of nicotinamide adenine dinucleotide, ADP: adenosine diphosphate, AMP: adenosine monophosphate. (For interpretation of the references to colour in this figure legend, the reader is referred to the web version of this article.)

Pearson analysis. There were 24 metabolites in group I. Among them, four kinds of organic carbon, namely 3R-aminononanoic acid, phenylglyoxylic acid, urocanic acid, and alpha-linolenic acid showed higher abundance in S1, which were carboxylic acid or carboxylic derivatives (Kaplan et al., 2016; Koshechko et al., 2002; Podsiadly, 2008) and have been observed to be important components of humic and fulvic acids (DiDonato and Hatcher, 2017). Therefore, humic and fulvic acids were detected in full denitrification (S1) due to the up-regulated carboxylic acid metabolism. Because of the difference in carbon metabolic pathways between anammox bacteria and denitrifiers (Acetyl-CoA pathway in anammox bacteria) (Strous et al., 2006), the tricarboxylic acid cycle in higher abundance of denitrifiers could account for up-regulated carboxylic acid metabolism in H_2-denitrification (Ren et al., 2021).

There were only six metabolites in group II, including gamma-glutamyl-S-methylcysteinyl-beta-alanine (S-methylhGSH), ethynodiol diacetate, 16B-Hydroxyestrone, flavidulol A, ginsenoyne J, and 17-beta-Estradiol-2,3-quinone. The levels of these metabolites were elevated in S2 compared with S1. S-methylhGSH showed the highest variable importance in the projection (VIP) among top-30 metabolites, presenting an important role in H_2-PDA. Ammonia can be removed in the form of alanine (Borsakova et al., 2022). S-methylhGSH as a product of nitrogen fixation was reported to be accumulated in *Phaseolus vulgaris* (Liao et al., 2013). Furthermore, proteins in bacteria might bind the intermediates to keep them from diffusing out (Akram et al., 2019), thus the adduct of S-methylhGSH with NH_4^+ promoted the removal of NH_4^+-N in wastewater.

3.4.2. Key metabolic pathways reveal the growth discrepancies

Changes in the metabolic state showed great discrepancies among anammox, denitrification and H_2-PDA in this study. H_2-PDA showed a unique metabolic pathway, unlike the combination of denitrification and anammox. The metabolites in this study were involved in energy, inorganic carbon fixing, nitrogen, and sulfur metabolism (Fig. 5), in agreement with earlier reports (Feng et al., 2018; Saboori-Robat et al., 2019). Adenosine diphosphate (ADP), together with adenosine monophosphate (AMP), are critical components of cellular energy metabolism (Russ et al., 2012). Compared with S1 and S2, ADP and AMP were significantly up-regulated in anammox bacteria (An), indicating that the anammox inoculum was rather active. Compared with An, the biofilm activity in MBfR (S1 and S2) was lower, which may be due to the shorter incubation time compared to the anammox inoculum (Gu et al., 2018). Metabolites in the Calvin cycle such as Ribose 1-phosphate, Glycerone-P, Glycerate-3P, and Glyceraldehyde-3P, which play important roles in inorganic carbon fixing, were down-regulated during full denitrification (S1). This was due to the lower concentration of total nitrogen in S1, which also showed lower biomass synthesis flux (0.009 e^- eq/(m^2·d)) compared to S2 (0.021 e^- eq/(m^2·d)) (Fig. 2d). Additionally, sulfur amino acids metabolites were also detected, including L-serine, cysteine, homoglutathione, L-methionine, S-methylhGSH, and *N*-acetyl-glucosamine. These compounds are closely associated with sulfur and nitrogen fixation (Saboori-Robat et al., 2019). Glutamate metabolism has been proven to be an important pathway for NH_4^+-assimilation (Jin et al., 2019), suggesting that the up-regulation of glutamate metabolism resulted in high NH_4^+-N removal in S2.

3.5. Environmental implications of H_2-PDA process

Results obtained in this study demonstrated that the H_2-PDA could be achieved successfully for advanced nitrogen removal without any organic carbon sources. The unbalanced growth of heterotrophic denitrifiers and autotrophic anammox bacteria can be avoided in H_2-PDA process. Furthermore, H_2-PDA theoretically saves 60 % H_2 over full H_2-denitrification (Pang et al., 2022). H_2 can be generated on site by reforming natural gas, which is much less expensive than acetate, ethanol, and glucose. For example, the cost of hydrogen is about 0.2 \$/kg NO_3^--N less than that of sodium acetate (Rittmann and McCarty, 2020). An MBfR is suitable for H_2 supply for its safety and efficiency. The residual H_2 gas in the headspace hydrogen was lower enough to preclude having an explosive air (Zhang et al., 2009). Although the functional bacteria and the metabolic properties were revealed in this study, there are still knowledge gaps on the interaction mechanisms between the various groups of bacteria. Therefore, further understanding on microbial mechanism is needed in future study.

4. Conclusions

In this study, a stable H_2-PDA process in MBfR inoculated with denitrifying and anammox bacteria achieved efficient and simultaneous removal of NO_3^--N (95.4 %) and NH_4^+-N (99.5 %). During H_2-PDA process, partial denitrification and anammox contributed to TN removal by 93.7 % and 6.3 %, respectively. *Meiothermus* was the key genus in partial denitrification, and *Candidatus_Brocadia* was predominant in TN removal. The up-regulation of the glutamate and gamma-glutamyl-S-methylcysteinyl-beta-alanine metabolism pathways played a key role in TN removal. Collectively, these findings demonstrated that implementing the low-cost H_2-PDA process in MBfRs provides an alternative for advanced wastewater treatment in the future.

CRediT authorship contribution statement

Si Pang: Conceptualization, Methodology, Software, Writing – original draft. **Yun Zhou:** Validation, Writing – review & editing. **Lin Yang:** Resources, Software. **Jingzhou Zhou:** Resources, Formal analysis. **Xiaodi Li:** Resources, Data curation. **Siqing Xia:** Project administration, Funding acquisition.

Declaration of Competing Interest

The authors declare that they have no known competing financial interests or personal relationships that could have appeared to influence the work reported in this paper.

Data availability

Data will be made available on request.

Acknowledgments

This work was supported by the National Key Project of Research and Development Plan of China [grant number 2021YFC3201300] and the National Natural Science Foundation of China [grant number NSFC 51678422].

Appendix A. Supplementary data

Supplementary data to this article can be found online at https://doi.org/10.1016/j.biortech.2022.128443.

References

Akram, M., Reimann, J., Dietl, A., Menzel, A., Versantvoort, W., Kartal, B., Jetten, M.S. M., Barends, T.R.M., 2019. A nitric oxide?binding heterodimeric cytochrome c complex from the anammox bacterium Kuenenia stuttgartiensis binds to hydrazine synthase. J. Biol. Chem. 294 (45), 16712–16728.

APHA. 2017. Standard Methods for the Examination of Water and Wastewater (23rd end.), American Public Health Association (APHA), American Water Works Association (AWWA), and Water Environment Federation (WEF). Washington, DC, USA.

Averill, B.A., Tiedje, J.M., 1982. The chemical mechanism of microbial denitrification. FEBS Lett. 138 (1), 8–12.

Bai, Y.H., Su, J.F., Ali, A., Chang, Q., Gao, Z.H., Wang, Y., Liu, Y., 2022. Insights into the mechanism of Mn(II)-based autotrophic denitrification: Performance, genomic, and metabonomics. Sci. Total Environ. 810.

Borsakova, D.V., Koleva, L.D., Protasov, E.S., Ataullakhanov, F.I., Sinauridze, E.I., 2022. Ammonium removal by erythrocyte-bioreactors based on glutamate dehydrogenase

from Proteus sp. jointly with porcine heart alanine aminotransferase. Sci. Rep. 12 (1).
Cai, X., Wang, Z.B., Qian, Y.C., Wang, A.Q., Yang, Y.F., Xia, S.Q., 2022. Comprehensively understanding fouling properties of cake and bulk sludge in an anammox membrane bioreactor: Focusing on the composition, interfacial thermodynamics and microbial community. J. Environ. Chem. Eng. 10 (6).
Cao, S.B., Du, R., Li, B.K., Wang, S.Y., Ren, N.Q., Peng, Y.Z., 2017. Nitrite production from partial-denitrification process fed with low carbon/nitrogen (C/N) domestic wastewater: performance, kinetics and microbial community. Chem. Eng. J. 326, 1186–1196.
Chen, F.M., Li, X., Gu, C.W., Huang, Y., Yuan, Y., 2018. Selectivity control of nitrite and nitrate with the reaction of S-0 and achieved nitrite accumulation in the sulfur autotrophic denitrification process. Bioresour. Technol. 266, 211–219.
Cheng, Y.F., Zhang, Z.Z., Li, G.F., Zhang, Q., Zheng, X.P., Cai, S., Xue, Y., Huang, B.C., Jin, R.C., 2020. Anammox granules acclimatized to mainstream conditions can achieve a volumetric nitrogen removal rate comparable to sidestream systems. Environ. Sci. Technol. 54 (20), 12959–12966.
Chu, Z.R., Wang, K., Li, X.K., Zhu, M.T., Yang, L., Zhang, J., 2015. Microbial characterization of aggregates within a one-stage nitritation-anammox system using high-throughput amplicon sequencing. Chem. Eng. J. 262, 41–48.
DiDonato, N., Hatcher, P.G., 2017. Alicyclic carboxylic acids in soil humic acid as detected with ultrahigh resolution mass spectrometry and multi-dimensional NMR. Org Geochem. 112, 33–46.
Dong, K., Feng, X.H., Wang, W.B., Chen, Y.C., Hu, W., Li, H.X., Wang, D.Q., 2021. Simultaneous partial nitrification and denitrification maintained in membrane bioreactor for nitrogen removal and hydrogen autotrophic denitrification for further treatment. Membranes 11 (12).
Du, R., Cao, S.B., Wang, S.Y., Niu, M., Peng, Y.Z., 2016. Performance of partial denitrification (PD)-ANAMMOX process in simultaneously treating nitrate and low C/N domestic wastewater at low temperature. Bioresour. Technol. 219, 420–429.
Du, R., Cao, S.B., Li, X.C., Wang, J.C., Peng, Y.Z., 2020a. Efficient partial-denitrification/anammox (PD/A) process through gas-mixing strategy: System evaluation and microbial analysis. Bioresour. Technol. 300.
Du, R., Cao, S.B., Zhang, H.Y., Peng, Y.Z., 2020b. Formation of partial-denitrification (PD) granular sludge from low-strength nitrate wastewater: The influence of loading rates. J. Hazard. Mater. 384.
Feng, Y., Zhao, Y.P., Guo, Y.Z., Liu, S.T., 2018. Microbial transcript and metabolome analysis uncover discrepant metabolic pathways in autotrophic and mixotrophic anammox consortia. Water Res. 128, 402–411.
Gong, L.X., Huo, M.X., Yang, Q., Li, J., Ma, B., Zhu, R.L., Wang, S.Y., Peng, Y.Z., 2013. Performance of heterotrophic partial denitrification under feast-famine condition of electron donor: A case study using acetate as external carbon source. Bioresour. Technol. 133, 263–269.
Gu, Z.L., Li, Y., Yang, Y.F., Xia, S.Q., Hermanowicz, S.W., Alvarez-Cohen, L., 2018. Inhibition of anammox by sludge thermal hydrolysis and metagenomic insights. Bioresour. Technol. 270, 46–54.
Guven, D., Dapena, A., Kartal, B., Schmid, M.C., Maas, B., van de Pas-Schoonen, K., Sozen, S., Mendez, R., Op den Camp, H.J.M., Jetten, M.S.M., Strous, M., Schmidt, I., 2005. Propionate oxidation by and methanol inhibition of anaerobic ammonium-oxidizing bacteria. Appl. Environ. Microbiol. 71 (2), 1066–1071.
Hou, X.L., Liu, S.T., Zhang, Z.T., 2015. Role of extracellular polymeric substance in determining the high aggregation ability of anammox sludge. Water Res. 75, 51–62.
Jia, F.X., Yang, Q., Liu, X.H., Li, X.Y., Li, B.K., Zhang, L., Peng, Y.Z., 2017. Stratification of extracellular polymeric substances (EPS) for aggregated anammox microorganisms. Environ. Sci. Technol. 51 (6), 3260–3268.
Jiang, Y., Chu, N., Qian, D.K., Zeng, R.J., 2020. Microbial electrochemical stimulation of caproate production from ethanol and carbon dioxide. Bioresour. Technol. 295.
Jin, P., Chen, Y.Y., Yao, R., Zheng, Z.W., Du, Q.Z., 2019. New insight into the nitrogen metabolism of simultaneous heterotrophic nitrification-aerobic denitrification bacterium in mRNA expression. J. Hazard. Mater. 371, 295–303.
Kaplan, H.M., Izol, V., Aridogan, I.A., Olgan, E., Yegani, A.A., Pazarci, P., Singirik, E., 2016. Protective effect of alpha-linolenic acid on gentamicin induced nephrotoxicity in mice. Int. J. Pharmacol. 12 (5), 562–566.
Kiskira, K., Papirio, S., van Hullebusch, E.D., Esposito, G., 2017. Influence of pH, EDTA/Fe(II) ratio, and microbial culture on Fe(II)-mediated autotrophic denitrification. Environ. Sci. Pollut. Res. 24 (26), 21323–21333.
Koshechko, V.G., Titov, V.E., Lopushanskaya, V.A., 2002. Electrochemical carboxylation of benzoyl bromide as effective phenylglyoxylic acid synthesis route. Electrochem. Commun. 4 (8), 655–658.
Kuenen, J.G., 2008. Anammox bacteria: from discovery to application. Nat. Rev. Microbiol. 6 (4), 320–326.
Lai, C.Y., Lv, P.L., Dong, Q.Y., Yeo, S.L., Rittmann, B.E., Zhao, H.P., 2018. Bromate and nitrate bioreduction coupled with poly-beta- hydroxybutyrate production in a methane-based membrane biofilm reactor. Environ. Sci. Technol. 52 (12), 7024–7031.
Li, J.L., Peng, Y.Z., Yang, S.H., Li, S., Feng, W.Y., Li, X.Y., Zhang, Q., Zhang, L., 2022. Successful application of anammox using the hybrid autotrophic-heterotrophic denitrification process for low-strength wastewater treatment. Environ. Sci. Technol. 56 (19), 13964–13974.
Liao, D., Cram, D., Sharpe, A.G., Marsolais, F., 2013. Transcriptome profiling identifies candidate genes associated with the accumulation of distinct sulfur gamma-glutamyl dipeptides in Phaseolus vulgaris and Vigna mungo seeds. Front. Plant Sci. 4.
Lu, Z.Y., Fu, J.J., Ma, Y.L., Jin, R.C., Fan, N.S., 2021. Response of anammox granules to the simultaneous exposure to macrolide and aminoglycoside antibiotics: Linking performance to mechanism. J. Environ. Manage. 286.
Moreno-Vivian, C., Cabello, P., Martinez-Luque, M., Blasco, R., Castillo, F., 1999. Prokaryotic nitrate reduction: Molecular properties and functional distinction among bacterial nitrate reductases. J. Bacteriol. 181 (21), 6573–6584.
Pang, S., Rittmann, B.E., Wu, C., Yang, L., Zhou, J., Xia, S., 2022. Synergistic inorganic carbon and denitrification genes contributed to nitrite accumulation in a hydrogen-based membrane biofilm reactor. Bioengineering 9 (5), 222.
Perna, V., Baum, A., Ernst, H.A., Agger, J.W., Meyer, A.S., 2019. Laccase activity measurement by FTIR spectral fingerprinting. Enzyme Microb. Technol. 122, 64–73.
Podsiadly, H., 2008. Interaction of vanadium(III) with imidazole carboxylic acids. Polyhedron 27 (6), 1563–1572.
Ren, T., Chi, Y.L., Wang, Y., Shi, X., Jin, X., Jin, P.K., 2021. Diversified metabolism makes novel Thauera strain highly competitive in low carbon wastewater treatment. Water Res. 206.
Rittmann, B.E., McCarty, P.L., 2020. Environmental Biotechnology: Principles and Applications, 2nd ed. McGraw-Hill Companies Inc, New York.
Russ, L., Harhangi, H.R., Schellekens, J., Verdellen, B., Kartal, B., Op den Camp, H.J.M., Jetten, M.S.M., 2012. Genome analysis and heterologous expression of acetate-activating enzymes in the anammox bacterium Kuenenia stuttgartiensis. Arch. Microbiol. 194 (11), 943–948.
Saboori-Robat, E., Joshi, J., Pajak, A., Solouki, M., Mohsenpour, M., Renaud, J., Marsolais, F., 2019. Common bean (Phaseolus vulgaris L.) accumulates most S-methylcysteine as its -glutamyl dipeptide. Plants-Basel 8 (5).
Schmid, M., Walsh, K., Webb, R., Rijpstra, W.I.C., van de Pas-Schoonen, K., Verbruggen, M.J., Hill, T., Moffett, B., Fuerst, J., Schouten, S., Damste, J.S.S., Harris, J., Shaw, P., Jetten, M., Strous, M., 2003. Candidatus "Scalindua brodae", sp nov., Candidatus "Scalindua wagneri", sp nov., two new species of anaerobic ammonium oxidizing bacteria. Syst. Appl. Microbiol. 26 (4), 529–538.
Strous, M., Pelletier, E., Mangenot, S., Rattei, T., Lehner, A., Taylor, M.W., Horn, M., Daims, H., Bartol-Mavel, D., Wincker, P., Barbe, V., Fonknechten, N., Vallenet, D., Segurens, B., Schenowitz-Truong, C., Medigue, C., Collingro, A., Snel, B., Dutilh, B. E., Op den Camp, H.J.M., van der Drift, C., Cirpus, I., van de Pas-Schoonen, K.T., Harhangi, H.R., van Niftrik, L., Schmid, M., Keltjens, J., van de Vossenberg, J., Kartal, B., Meier, H., Frishman, D., Huynen, M.A., Mewes, H.W., Weissenbach, J., Jetten, M.S.M., Wagner, M., Le Paslier, D., 2006. Deciphering the evolution and metabolism of an anammox bacterium from a community genome. Nature 440 (7085), 790–794.
Tang, Y.N., Zhou, C., Ziv-El, M., Rittmann, B.E., 2011. A pH-control model for heterotrophic and hydrogen-based autotrophic denitrification. Water Res. 45 (1), 232–240.
Tautenhahn, R., Cho, K., Uritboonthai, W., Zhu, Z.J., Patti, G.J., Siuzdak, G., 2012. An accelerated workflow for untargeted metabolomics using the METLIN database. Nat. Biotechnol. 30 (9), 826–828.
Van Ginkel, S.W., Kim, B.O., Yang, Z.M., Sittmann, R., Sholin, M., Micelli, J., Rittmann, B.E., 2012. Effect of NaCl on nitrate removal from ion-exchange spent brine in the membrane biofilm reactor (MBfR). Water Sci. Technol. 65 (1), 100–104.
Wrighton, K.C., Agbo, P., Warnecke, F., Weber, K.A., Brodie, E.L., DeSantis, T.Z., Hugenholtz, P., Andersen, G.L., Coates, J.D., 2008. A novel ecological role of the Firmicutes identified in thermophilic microbial fuel cells. ISME J. 2 (11), 1146–1156.
Xia, S.Q., Wu, C.Y., Yang, X.X., Zhou, Y., Zhou, L.M., Ran, Y.J., Rittmann, B.E., 2020. Bioreduction of nitrate in high-sulfate water using a hydrogen-based membrane biofilm reactor equipped with a separate carbon dioxide module. Chem. Eng. J. 385.
Yuan, H.G., Huang, S., Yuan, J.Q., You, Y.Y., Zhang, Y.Q., 2021. Characteristics of microbial denitrification under different aeration intensities: Performance, mechanism, and co-occurrence network. Sci. Total Environ. 754.
Yuan, Y., Li, X., Li, W., Shi, M., Zhang, M., Xu, P.L., Li, B.L., Huang, Y., 2022. Effects of different reduced sulfur forms as electron donors in the start-up process of short-cut sulfur autotrophic denitrification . Bioresource Technol. 354.
Zhang, J.W., Peng, Y.Z., Li, X.C., Du, R., 2022. Feasibility of partial-denitrification/anammox for pharmaceutical wastewater treatment in a hybrid biofilm reactor. Water Res. 208.
Zhang, Y.H., Zhong, F.H., Xia, S.Q., Wang, X.J., Li, J.X., 2009. Autohydrogenotrophic denitrification of drinking water using a polyvinyl chloride hollow fiber membrane biofilm reactor. J. Hazard. Mater. 170 (1), 203–209.